ACCSCIENCE PUBLISHING

Engineering Science in Additive Manufacturing

ORIGINAL RESEARCH ARTICLE

Impact of machine factors on the surface quality of parts fabricated via powder bed fusion

Zhen Lu[1], Ming Jen Tan[1]*, Yi Zhang[2], Jia An[3], and Chee Kai Chua[3]

[1]Singapore Centre for 3D Printing, Nanyang Technological University, Singapore

[2]School of Integrated Circuit Science and Engineering, University of Electronic Science and Technology of China, Sichuan, China

[3]Engineering Product Development Pillar, Singapore University of Technology and Design, Singapore

Abstract

In the growing additive manufacturing industry, there is increasing demand for improved as-built surface quality of parts fabricated by the powder bed fusion (PBF) process, particularly in the aerospace, medical, and tooling industrial sectors. The surface finish of PBF parts is often suboptimal due to the inherent layer-by-layer fabrication process. Depending on the material used, the average surface roughness (Ra) of PBF components typically ranges from 5 to 50 μm. To address this issue, various strategies have been investigated, including optimizing printing process parameters, refining support designs, and upgrading laser hardware. In this study, we investigated the machine factors on the as-built surface quality of parts in the PBF process. Fully dense as-built 1.2709 tool steel parts were produced with a relative density of 99.9% using platform pre-heating. Without heat treatment, the as-built part exhibited an ultimate tensile strength of 1,135 ± 75 MPa, yield strength of 915 ± 120 MPa, and an elongation of 12 ± 3%. Vickers hardness was measured at 339 ± 35. Surface measurements were performed on parts placed across the substrate plate, with the Ra of as-built vertical walls averaging 22.6 ± 11.9 mm. Results showed that the surface quality of as-built 1.2709 tool steel parts, with a layer thickness of 30 μm, was significantly affected by their distance from the inert gas outlet and the laser center. This study demonstrates that the as-built surface quality of PBF parts can be controlled through more effective build job preparation without changing key processing parameters.

Keywords: Additive manufacturing; 3D printing; Powder bed fusion; Selective laser melting; Surface quality; Tool steel

***Corresponding author:**
Ming Jen Tan
(mmjtan@ntu.edu.sg)

Citation: Lu Z, Tan MJ, Zhang Y, An J, Chua CK. Impact of machine factors on the surface quality of parts fabricated via powder bed fusion. *Eng Sci Add Manuf*. 2025;1(2):025240014. doi: 10.36922/ESAM025240014

Received: May 13, 2055

Revised: June 14, 2025

Accepted: June 18, 2025

Published online: June 24, 2025

1. Introduction

Additive manufacturing (AM), as defined by International Standardization Organization/ASTM 52900:2021,[1] is the process of joining materials to make parts from 3D model data. Usually, materials are joined layer upon layer, as opposed to subtractive and formative methods of manufacturing. Seven families of AM are commonly recognized, while powder bed fusion (PBF) uses lasers as the energy source to fully melt and fuse the metal powder materials directly to form the near-net shape metal product, which can be fully functional.

Laser-based PBF of metals, commonly known as selective laser melting (SLM) or direct metal laser sintering, is an AM process capable of producing near-net-shape metal components for research and industrial applications. The process begins with a computer-aided design model configured with process parameters and sliced into layers using specialized software. During fabrication, metal powder is deposited onto a build plate layer-by-layer with a predefined layer thickness.[2] The laser selectively melts the powder in each layer, fusing it to form the final part.[3] PBF enables the rapid fabrication of metal components with complex geometries, offering good quality and dimensional accuracy.[4] It enhances design freedom by eliminating many of the geometric constraints imposed by conventional machining methods. In addition, PBF supports part integration, which can reduce manufacturing costs and improve overall component performance, making it well-suited for meeting industrial demands.[5] Parts are built layer-by-layer with the thickness of each layer at 20 – 100 μm. Ideal metal powder is spherical, medium-sized, with a narrow particle distribution. Oxygen level is controlled at <500 ppm. The platform can be heated up to 200°C.[6] PBF technology is compatible with many materials, highly efficient, and capable of producing complex end-products of high precision.[7,8] Companies such as General Electric, Airbus, Boeing, and Rolls-Royce are all at the forefront of using more metal AM in their production line.[9-11]

Key advantages of the PBF process include greater design freedom, enhanced functionality, reduced tooling and setup costs, lightweight structures, mass customization, and overall cost savings.[8] However, various post-processing steps, such as heat treatment, secondary machining, and polishing, are often necessary to improve the quality of parts produced by the PBF process further. Components fabricated using PBF can exhibit superior properties compared to those made by conventional methods, largely due to the refined microstructures formed during the rapid cooling and solidification cycles, with cooling rates ranging from 10^3 to 10^6°C/s. Despite its potential for producing near-net-shape components, PBF technology has yet to be widely adopted across industries. A key barrier to broader implementation is the need for additional post-processing to achieve the surface quality required for many applications.[12]

The surface roughness (Ra, the arithmetic mean deviation of the assessed profile) of metal additive manufacturing (AM) components varies between 5 and 50 μm, depending on the material used.[12] At present, additional post-processes such as computer numerical control milling and turning, grinding, and polishing are implemented to achieve <1 μm Ra.[13] In addition, the following factors are important in determining the final surface quality built by PBF: Material feedstock (type, size, and quality), surface orientation concerning the process, support interface, and key processing parameters.[14] In recent years, the effect of machine factors on Ra variation has also received attention.

A variety of process parameters influence print quality in AM, including laser power, scanning speed, hatch spacing, layer thickness, scanning strategy, spot size, and pre-heat temperature.[15] In addition, other factors, such as gas flow rate and raw material properties, can impact process stability and overall print quality. These parameters collectively affect mass and heat transfer within the melt pool, thereby influencing melt pool behavior and the resulting part quality.[16] Meanwhile, heat treatment such as annealing also has a major effect on the fracture toughness and the threshold for fatigue crack initiation.[17] Two other parameters to be considered are scanning strategy and build orientation.[18]

The main characteristics of 1.2709 tool steel are characterized by high hardness and high ductility.[19-22] Its specific mechanical properties allow usage in high-stress components due to its high wear resistance.[23-25] Lasers can also be used to diminish the Ra of 1.2709 tool steel PBF parts up to 41% and increase their hardness up to 88%.[26] The maximum operating temperatures can further reduce wear. It is commonly used for applications such as conformal cooling systems for mold devices.[27,28] Various build strategies were developed to optimize the printing process of 1.2709 tool steel.[29-33] In hybrid manufacturing applications, 1.2709 tool steel (ASTM A276/M300) is widely used and adopted.[34-36] Its performance can also be enhanced via various heat treatment methods, such as solution annealing and aging after the PBF fabrication process.[37,38] Its microstructure change during heat treatment was investigated to obtain the optimal heat treatment process.[39-42]

This study aims to produce high-quality PBF parts and investigate the machine factors affecting the surface quality of as-built parts from the PBF process, such as inert gas flow and the position of parts relative to the location of the laser spot center.

2. Data and methods

2.1. Material and manufacturing

This study used 1.2709 tool steel (ASTM A276/M300) (Nikon SLM Solutions AG, Germany). As shown in Figure 1, the powder has a spherical morphology according to the standards of the German Institute for Standardization (DIN), European Standard (EN),

and International Standardization Organization (ISO) 3252:2023, with a particle size distribution of 10 – 45 μm. Its mass density is 8.0 g/cm^3. Its chemical composition is shown in Table 1. The powder was dried before loading into the PBF machine with professional dry bags (Nikon SLM Solutions AG, Germany) to ensure that the relative humidity of the powder was <10% before starting the PBF process.

An AM machine was used for the PBF process (SLM280 Twin 700W laser, Nikon SLM Solutions, Germany). A powder layer thickness of 30 μm was maintained, with a rotating hatch angle of 67°, whereas the laser beam focus diameter was 80 – 115 μm. The substrate plate was pre-heated to 200°C before starting the fabrication process. During the fabrication process, its gas flow came from right to left, and the recoating direction came forward and backward (Figure 2). High-purity argon gas was pumped into the build chamber to maintain oxygen level below 1,000 ppm throughout the fabrication process. Argon gas flow speed was controlled at 22 m/s to ensure that heavy spattering and soot formed from the rapid melting process could be effectively removed from the powder bed. The oxygen level was closely monitored via the AM system's monitoring control system to ensure that the oxygen level was below 1,000 ppm. The metal powder was spread onto the substrate plate evenly with the calibrated recoater. The gap between the recoater blade and the substrate plate was controlled at 200 μm to ensure consistency across build jobs. Steel substrate plates were also ground smoothly, with their Ra <30 μm, to ensure that the building of the first layer on the substrate plate was smooth.

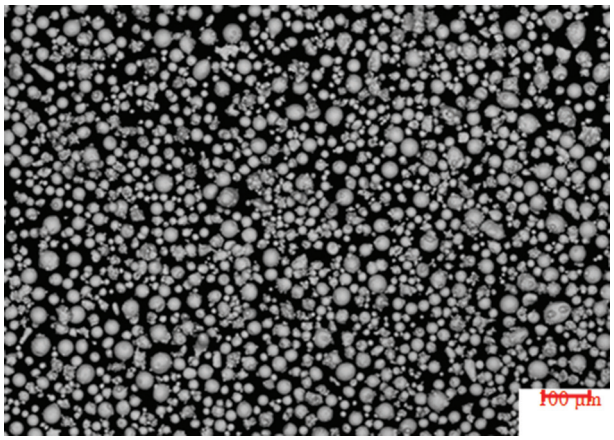

Figure 1. Powder characteristics of 1.2709 tool steel (ASTM A276/M300) metal powder. Scale bar: 100 μm; magnification: ×100.

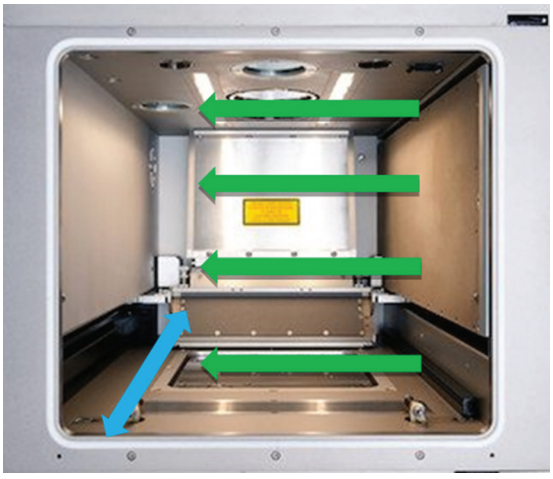

Figure 2. Gas flow and recoating direction of Nikon SLM Solutions' SLM280 twin laser additive manufacturing system.
Note: Green arrows indicate the gas flow direction, and blue arrow indicates the recoating direction.

2.2. Design of parts

In this study, the testing parts in Figure 3 were produced and measured for their surface quality. Each part consisted of a 25 × 25 × 10 mm^3 cube with a 25 mm diameter, 10 mm high cylinder on top. Twenty parts were produced per plate. The parts were removed from the substrate plate for further measurements of their surface quality. Surface quality was measured on the front, back, left, and right surfaces of every cube. Eighty measurements were performed to investigate the surface quality of as-built PBF parts against gas flow direction, recoat direction, and consistency across the full plate. The parts were stored inside sealed boxes during transportation to minimize the contamination of the part surface from the atmosphere.

2.3. Experimental and characterization methods

In this study, a 3D laser scanning microscope (VK-X200 series, KEYENCE, Japan) was used. On every surface, a 1 mm × 1 mm surface area was measured. Relative density was determined by testing specimens using light microscopy. Tensile testing was performed following the standards of DIN, EN, and ISO 6892 – 1:2020 B and conducted at room temperature. Tensile parts were processed before testing (geometry according to the standards of DIN, EN 50125:2016 – D6 × 30, and DIN 50125:2016 – C6 × 30). Hardness testing was conducted according to the standards

Table 1. Chemical composition of 1.2709 tool steel powder (mass fraction in %)

Element	Fe	Ni	Co	Mo	Ti	Al	Mn	Si	C
%	Balance	18.00 – 19.00	8.50 – 9.50	4.70 – 5.20	0.50 – 0.80	0.05 – 0.15	0.10	0.10	0.03

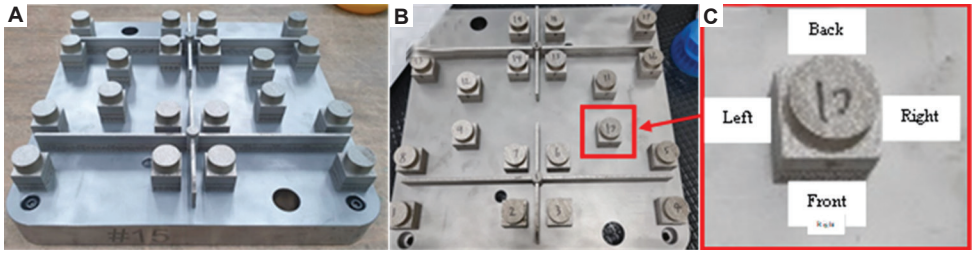

Figure 3. As-built parts are produced using the powder bed fusion system. (A) As-built parts on the substrate plate; (B) parts with labeling from the top view; (C) front, back, left, and right surfaces of parts.

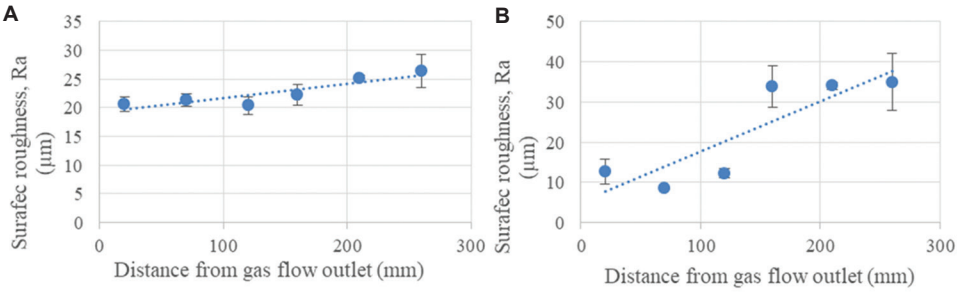

Figure 4. Surface roughness for surfaces against their distance to the gas flow outlet. (A) Overall surface. (B) left surface.

DIN, EN, and ISO 6507 – 1:2024. Measurement direction was "2" according to the Association of German Engineers (VDI) 3405 2.1.

3. Results and discussion

3.1. Mechanical properties

The results of the mechanical properties of this 1.2709 tool steel (ASTM A276/M300) metal powder produced from Nikon SLM Solutions' SLM280 twin laser AM system are shown in Table 2 after conducting respective density test, tensile test, and hardness test.

3.2. Surface quality properties

The overall average Ra of all 80 measurements in this study is 22.6 ± 11.9 μm. The average Ra of left, right, front, and back surfaces are 23.0 ± 15.3 μm, 24.5 ± 14.3 μm, 19.1 ± 6.9 μm, and 23.8 ± 9.2 μm, respectively. Detailed data of all measurements are shown in Table 3. All parts' right surfaces were the closest to the gas flow outlet, whereas their left surfaces were the furthest away from the gas flow outlet. Their front and back surfaces faced the recoater's moving direction when recoating metal powder during the PBF process.

3.3. Effect of gas flow

The effect of gas flow on surface quality was analyzed. Figure 4 and Table 4 show the change in Ra due to the change in its distance from the gas flow outlet. These results showed that the measured Ra increased gradually when the fabricated parts were placed further from the gas flow outlet. The impact of such gas flow became significant when the distance exceeded 200 mm. Ra of parts at a distance of 120 mm from the gas flow outlet was better than that at 70 mm. The potential root cause was that those parts placed at a distance of 120 mm from the gas flow outlet were closer to the center of the laser spot location. Therefore, such results also show that the distance of the part from the center of the laser position has a stronger impact on the as-built parts' Ra compared to the distance from the gas flow outlet.

Table 2. Mechanical properties of 1.2709 tool steel (ASTM A276/M300) used in this study

Properties	Values
Relative density	99.9%
Ultimate tensile strength (MPa)	1135±75
Yield strength (MPa)	915±120
Elongation (%)	12±3
Vickers hardness (HV10)	339±35

Table 3. Overall surface quality of all measurements

Surface direction	Surface roughness, Ra (μm)
Overall	22.6±11.9
Left	23.0±15.3
Right	24.5±14.3
Front	19.1±6.9
Back	23.8±9.2

The argon gas was blown from the inert gas outlet on the right of the build chamber. Spattering and soot were formed during the rapid laser melting process. Although most spattering and soot were expected to be blown away from the powder bed working area, a portion of this spattering and soot would still fall onto the powder bed, affecting the surface quality if it fell onto the edges of the fabricated parts. This issue became more significant for those parts placed on the left part of the building areas because more spattering and soot were generated from the right areas.

In addition, Figure 5 shows that the standard deviation of the Ra increases gradually when the distance to the gas flow outlet increases from 20.0 mm to 120.0, 160.0, and 260.0 mm, with the same number of measurements and parts at each location. When parts were placed further from the gas outlet, unpredictable spattering and soot would have a more significant impact on the parts' Ra. Moreover, while the argon gas flow speed was maintained inside the build chamber, its effectiveness in removing the spattering and soot decreased when the parts were further away from the gas outlet position. A sintered wall was used at the argon gas outlet to ensure a laminar flow was blown into the build chamber. Turbulence would still be formed in the chamber, especially in spaces further away from the gas flow outlet. Such turbulence would also bring some spattering and soot back to the powder bed in the left area, affecting the as-built parts' surface quality.

Table 4. Surface roughness for all surfaces against their distance to the gas flow outlet

Distance to gas flow outlet (mm)	Part number	Average surface roughness (μm)
20.0	4, 5, 16, 17	20.7±2.5
70.0	10, 11	21.4±2.1
120.0	3, 6, 15, 18	20.4±3.1
160.0	2, 7, 14, 19	22.3±3.5
210.0	9, 12	25.1±1.1
260.0	1, 8, 13, 20	26.4±5.7

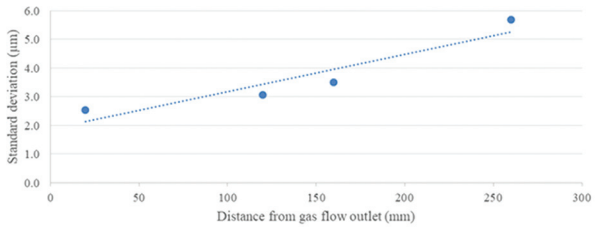

Figure 5. Standard deviation of the parts' surface roughness against their distance to the gas flow outlet

3.4. Effect of build position

The average Ra of each part is defined as the average value of its front, back, left, and right surfaces' Ra values (Equation I):

$$R_a\,(sample) = average\,(R_a[front] + R_a\,[back] + R_a\,[left] + R_a\,[right]) \quad (I)$$

In this study, a twin laser PBF system was used. The laser positions are marked as "X" in Figure 6. Detailed data of all 20 parts and their positions are shown in Figure 6. Parts placed near the center of the laser, such as parts 2, 3, 6, 7, 14, 15, 18, and 19, had a better surface quality in the range of 15 – 20 μm. Parts placed further away from the center of the laser, such as parts 1, 4, 8, and 13, had poorer surface quality in the range of 25 – 35 μm.

The effect of building positions was analyzed. Figure 7 and Table 5 show the average Ra compared to the distance of the fabricated parts from the center of the laser spot positions. Ra values of PBF fabricated parts increased gradually when the parts were placed further away from the center of the laser spot location.

When the parts were placed further away from the center of the laser spot, the laser spot became more

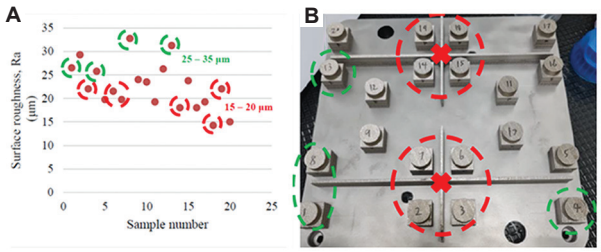

Figure 6. The position of parts in the build chamber and their overall surface quality. (A) Overall surface quality of the parts. (B) Positions of parts with labeling.
Note: The "X" marks in (B) indicate the laser position in the powder bed fusion system. Red circles indicate regions close to the center of the laser, whereas green circles indicate further regions. The parts included in rectangles in (A) correspond to the parts included in the circles of the same color in (B).

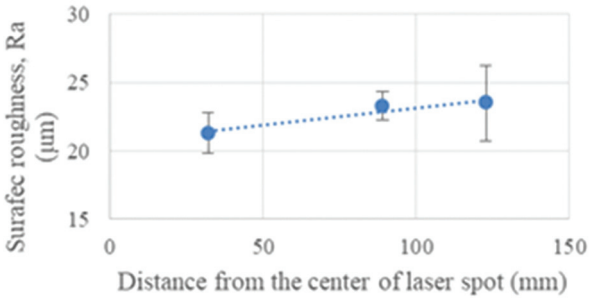

Figure 7. Surface roughness for all surfaces against their distance to the center of the laser spot

elliptical. This would result in reduced energy density, thus causing higher Ra or even forming porosity inside the part due to a lack of fusion. Figure 8 illustrates the consequence of such laser interaction due to the position of the parts. When the laser was shot directly onto the powder bed from 90° vertically, the melt pool and laser spot size were nearly a perfect round shape. However, when the part moved away from the center of the laser spot, the melt pool shape became distorted, which negatively affected the surface quality of the as-built parts.

3.5. Summary of the surface quality of parts

Figure 9 summarizes the measured surface quality of parts fabricated on different positions of the substrate plate, with the indication of the gas flow direction and recoating directions.

Table 5. Surface roughness for all surfaces against their distance to the center of the laser spot

Distance from the laser center (mm)	Part number	Average surface roughness (μm)
32.0	2, 3, 6, 7, 14, 15, 18, 19	21.3±3.0
89.0	9, 10, 11, 12	23.3±2.0
122.6	1, 4, 5, 8, 13, 16, 17, 20	23.5±5.5

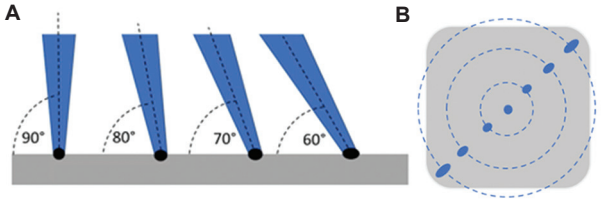

Figure 8. Illustration of laser interaction on the powder bed. (A) Laser interaction with powder bed at different incident angles. (B) Elliptical shape of the laser beam when the parts are placed at a different location on the substrate plate (courtesy Nikon SLM Solutions AG).

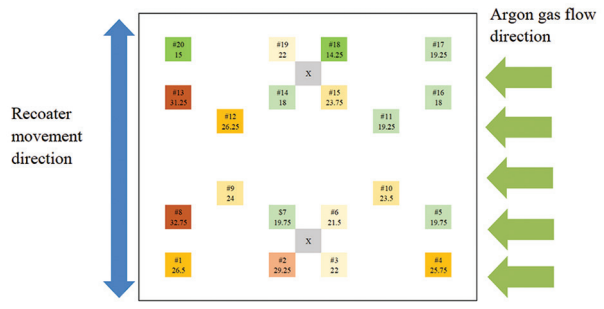

Figure 9. Surface roughness for all parts on the substrate plate.
Notes: # indicates part number. The "X" mark in gray indicates the center of the laser spot. Green boxes indicate that produced parts have a good Ra value smaller than 20 μm. Orange boxes indicate those produced parts have a relatively poor Ra value between 20 μm and 30 μm. Red boxes indicate those produced parts have a poor Ra value larger than 30 μm.

When all identical parts with the same geometry design and the same support design were fabricated inside the same build chamber, using the same argon gas settings, recoating settings, metal powder, and process parameters, their Ra varied across the full substrate plate. The key factors that account for such variations are the distance from the parts to the gas flow outlet and the center of the laser spot. For example, parts 1, 8, and 13 had the worst Ra because they were furthest away from the gas flow outlet, as well as the center of the laser spot. On the other hand, parts 5, 7, 11, 14, 16, 17, and 18 had better Ra because these parts were placed close to either the center of the laser spot or the gas flow outlets. As a general trend observed from the measurements, parts positioned on the right side of the substrate plate (which are closer to the gas flow outlet) and parts placed near the center of the laser spot have better Ra compared with those parts that are placed away from the gas flow outlet and the center of laser spot position.

4. Conclusion

In this study, 1.2709 tool steel (ASTM A276/M300) was fabricated using the PBF system. The main conclusions of the study are summarized as follows:

(i) Fully dense parts of a relative density of 99.9% were fabricated from the PBF process with platform pre-heating. Without heat treatment, its as-built ultimate tensile strength was 1,135 ± 75 MPa, yield strength was 915 ± 120 MPa, and elongation was 12 ± 3 %. It has HV10 at 339 ± 35.

(ii) Surface measurements were performed for parts placed across the substrate plate, and the average Ra for as-built vertical walls was 22.6 ± 11.9 μm.

(iii) Machine factors, such as the distance of parts to the gas flow outlet, impact the Ra of as-built parts. The Ra becomes higher when the parts are placed further away from the inert gas outlet. The distance of parts to the center of the laser spot also impacts the Ra of as-built parts. The Ra increases when the parts are placed further away from the center of the laser spot location.

This study provides guidance and reference for optimizing the PBF fabrication strategy, especially on the part placement, considering machine factors such as inert gas outlet and laser spot position.

Acknowledgments

The part fabrication work was supported by SLM Solutions Singapore Pte Ltd. The metal powder was supported by SLM Solutions Singapore Pte Ltd.

Funding

None.

Conflict of interest

The authors declare that they have no known competing financial interests or personal relationships that could have appeared to influence the work reported in this paper.

Author contributions

Conceptualization: Zhen Lu
Formal analysis: Zhen Lu
Investigation: Zhen Lu
Methodology: Zhen Lu
Writing – original draft: Zhen Lu
Writing – review & editing: All authors

Ethics approval and consent to participate

Not applicable.

Consent for publication

Not applicable.

Availability of data

The data presented in this study are available upon request from the corresponding author.

Further disclosure

Part of the findings have been presented in a conference titled "Impact of Machine Factors on the Surface Quality of Parts Fabricated by Selective Laser Melting," Materials Today: Proceedings (AMBW 2022), by Zhen Lu, Chee Kai Chua, Ming Jen Tan, Yi Zhang, and Jia An.

References

1. ISO/ASTM. *Additive Manufacturing -- General Principles -- Part 2: Overview of Process Categories and Feedstock, ISO Online Browsing Platform*; 2021. Available from: https://www.iso.org/obp/ui/#iso:std:iso-astm:52900:ed-2:v1:en [Last accessed on 2025 May 12].
2. Sing SL, Yeong WY, Wiria FE, *et al*. Direct selective laser sintering and melting of ceramics: A review. *Rapid Prototyp J*. 2017;23(3):611-623.
   doi: 10.1108/RPJ-11-2015-0178
3. Wong KV, Hernandez A. A review of additive manufacturing. *ISRN Mech Eng*. 2012;2012:208760.
   doi: 10.5402/2012/208760
4. Jiao L, Chua ZY, Moon SK, Song J, Bi G, Zheng H. Femtosecond laser produced hydrophobic hierarchical structures on additive manufacturing parts. *Nanomaterials*. 2018;8(8):601.
   doi: 10.3390/nano8080601
5. Yap CY, Chua CK, Dong ZL, *et al*. Review of selective laser melting: Materials and applications. *Appl Phys Rev*. 2015;2(4):041101.
   doi: 10.1063/1.4935926
6. Zhang B, Dembinski L, Coddet C. The study of the laser parameters and environment variables effect on mechanical properties of high compact parts elaborated by selective laser melting 316L powder. *Mater Sci Eng A*. 2013;584:21-31.
   doi: 10.1016/j.msea.2013.06.055
7. Zhang LC, Attar H. Selective laser melting of titanium alloys and titanium matrix composites for biomedical applications: A review. *Adv Eng Mater*. 2016;18(4):463-475.
   doi: 10.1002/adem.201500419
8. Tan JHK, Sing SL, Yeong WY. Microstructure modelling for metallic additive manufacturing: A review. *Virtual Phys Prototyp*. 2019;15(1):87-105.
   doi: 10.1080/17452759.2019.1677345
9. Boyer RR. An overview on the use of titanium in the aerospace industry. *Mater Sci Eng A*. 1996;213(1-2):103-114.
   doi: 10.1016/0921-5093(96)10233-1
10. Boyer RR. Applications of beta titanium alloys in airframes. *JOM*. 1993;45(7):33-46.
11. Boyer RR. Aerospace applications of beta titanium alloys. *JOM*. 1994;46(7):20-23.
12. Nagalingam AP, Yeo SH. Controlled hydrodynamic cavitation erosion with abrasive particles for internal surface modification of additive manufactured components. *Wear*. 2018;414-415:89-100.
   doi: 10.1016/j.wear.2018.08.006
13. Mumtaz K, Hopkinson N. Top surface and side roughness of Inconel 625 parts processed using selective laser melting. *Rapid Prototyp J*. 2009;15(2):96-103.
   doi: 10.1108/13552540910943397
14. Triantaphyllou A, Giusca CL, Macaulay GD, *et al*. Surface texture measurement for additive manufacturing. *Surf Topogr Metrol Prop*. 2015;3(2):024002.
   doi: 10.1088/2051-672X/3/2/024002
15. Nguyen HD, Pramanik A, Basak AK, *et al*. A critical review on additive manufacturing of Ti-6Al-4V alloy: Microstructure and mechanical properties. *J Mater Res Technol*. 2022;18:4641-4661.
   doi: 10.1016/j.jmrt.2022.04.055
16. Zhang B, Li Y, Bai Q. Defect formation mechanisms in selective laser melting: A review. *Chin J Mech Eng*. 2017;30:515-527.
   doi: 10.1007/s10033-017-0121-5
17. Belan J, Bokůvka O, Uhríčik M, Kuchariková L, Vaško A. The influence of quenching on fatigue life of Ti6Al4V alloy.

IOP Conf Ser Mater Sci Eng. 2021;1178:012006.

doi: 10.1088/1757-899X/1178/1/012006

18. Shipley H, McDonnell D, Culleton M, *et al*. Optimisation of process parameters to address fundamental challenges during selective laser melting of Ti-6Al-4V: A review. *Int J Mach Tools Manuf*. 2018;128:1-20.

doi: 10.1016/j.ijmachtools.2018.01.003

19. Żaba K, Balcerzak M, Kuczek Ł, *et al*. Application of powder-bed fusion of metals using a laser for manufacturing of M300 maraging steel tools intended for sheet metal bending. *Materials (Basel)*. 2024;17(24):6185.

doi: 10.3390/ma17246185

20. Raghuraman V, Kumar TS. The impact of different heat treatments on the surface characteristics, residual stresses, and tensile strength of maraging steel 1.2709 parts produced by LPBF. *Results Eng*. 2025;26:105509.

doi: 10.1016/j.rineng.2025.105509

21. Marchini L, Tonolini P, Montesano L, *et al*. The corrosion resistance of maraging steel 1.2709 produced by L-PBF in contact with molten Al-alloys. *Procedia Struct Integr*. 2024;53:203-211.

doi: 10.1016/j.prostr.2024.01.025

22. Sawicki J, Stachurski W, Kuryło P, *et al*. Comparative analysis of the dimensional accuracy and surface characteristics of gears manufactured using the 3D printing (DMLS) technique from 1.2709 steel. *Materials (Basel)*. 2025;18(7):1461.

doi: 10.3390/ma18071461

23. Asnafi N. Application of laser-based powder bed fusion for direct metal tooling. *Metals*. 2021;11(3):458.

doi: 10.3390/met11030458

24. Piekło J, Garbacz-Klempka A, Myszka D, Figurski K. Numerical and experimental analysis of strength loss of 1.2709 maraging steel produced by selective laser melting (SLM) under thermo-mechanical fatigue conditions. *Materials* (*Basel*). 2023;16(24):7682.

doi: 10.3390/ma16247682

25. Strakosova A, Průša F, Michalcová A, Kratochvíl P, Vojtěch D. Annealing response of additively manufactured high-strength 1.2709 maraging steel depending on elevated temperatures. *Materials (Basel)*. 2022;15(11):3753.

doi: 10.3390/ma15113753

26. Černašėjus O, Škamat J, Markovič V, *et al*. Surface laser processing of additive manufactured 1.2709 steel parts: Preliminary study. *Adv Mater Sci Eng*. 2019;2019:7029471.

doi: 10.1155/2019/7029471

27. Piekło J, Garbacz-Klempka A. Use of maraging steel 1.2709 for implementing parts of pressure mold devices with conformal cooling system. *Materials* (*Basel*). 2020;13(23):5533.

doi: 10.3390/ma13235533

28. Ravi S, Satheeshkumar V, Kumaran M. Mechanical properties and microstructure characterization of stainless steel 316L and maraging steel 1.2709 bimetallic structures fabricated by laser powder bed fusion. *J Mater Eng Perform*. 2025.

doi: 10.1007/s11665-025-11451-8

29. Jarfors AEW, Shashidhar ACGH, Yepur HK, Steggo J, Andersson NE, Stolt R. Build strategy and impact strength of SLM produced maraging steel (1.2709). *Metals*. 2021;11(1):51.

doi: 10.3390/met11010051

30. Jhabvala J, Boillat E, Antignac T, Glardon R. On the effect of scanning strategies in the selective laser melting process. *Virtual Phys Prototyp*. 2010;5(2):99-109.

doi: 10.1080/17452751003688368

31. Jägle EA, Choi PP, Van Humbeeck J, Raabe D. Precipitation and austenite reversion behavior of a maraging steel produced by selective laser melting. *J Mater Res*. 2014;29(17):2072-2079.

doi: 10.1557/jmr.2014.204

32. Hoseini SRE, Arabi H, Razavizadeh H. Improvement in mechanical properties of C300 maraging steel by application of VAR process. *Vacuum*. 2008;82(5):521-528.

doi: 10.1016/j.vacuum.2007.08.008

33. Hatos I, Hargitai H, Fekete G, Fekete I. Effect of energy density on the mechanical properties of 1.2709 maraging steel produced by laser powder bed fusion. *Materials (Basel)*. 2024;17(14):3432.

doi: 10.3390/ma17143432

34. Kumaran M, Ravi S. Influence of hybrid additive manufacturing processes on the microstructure and mechanical properties of maraging steel 1.2709 components with post-processing heat treatments. *Mater Lett*. 2024;377:137427.

doi: 10.1016/j.matlet.2024.137427

35. Vinoth V, Kumaran M, Ravi S. Investigation of heat treatment effects on hybrid manufacturing of stainless steel 316L components using directed energy deposition: Microstructural and tensile behavior analysis. *J Mater Eng Perform*. 2025.

doi: 10.1007/s11665-025-11023-w

36. Kučerová L, Zetková I, Jeníček Š, Burdová K. Production of hybrid joints by selective laser melting of maraging tool steel 1.2709 on conventionally produced parts of the same steel. *Materials* (*Basel*). 2021;14(9):2105.

doi: 10.3390/ma14092105

37. Simm TH, Sun L, Galvin DR, *et al*. The effect of a two-stage heat-treatment on the microstructural and mechanical properties of a maraging steel. *Materials* (*Basel*). 2017;10(12):1346.

doi: 10.3390/ma10121346

38. Monkova K, Zetkova I, Kučerová L, *et al*. Study of 3D printing direction and effects of heat treatment on mechanical properties of MS1 maraging steel. *Arch Appl Mech*. 2019;89:791-804.

doi: 10.1007/s00419-018-1389-3

39. Mutua J, Nakata S, Onda T, Chen ZC. Optimization of selective laser melting parameters and influence of post heat treatment on microstructure and mechanical properties of maraging steel. *Mater Des*. 2018;139:486-497.

doi: 10.1016/j.matdes.2017.11.042

40. Tan C, Zhou K, Ma W, Zhang P, Liu M, Kuang T. Microstructural evolution, nanoprecipitation behavior and mechanical properties of selective laser melted high-performance grade 300 maraging steel. *Mater Des*. 2017;134:23-34.

doi: 10.1016/j.matdes.2017.08.026

41. Mooney B, Kourousis KI, Raghavendra R. Plastic anisotropy of additively manufactured maraging steel: Influence of the build orientation and heat treatments. *Addit Manuf*. 2019;25:19-31.

doi: 10.1016/j.addma.2018.10.032

42. Bai Y, Yang Y, Wang D, Zhang M. Influence mechanism of parameters process and mechanical properties evolution mechanism of maraging steel 300 by selective laser melting. *Mater Sci Eng A*. 2017;703:116-123.

doi: 10.1016/j.msea.2017.06.033